Available online at www.sciencedirect.com
SCIENCE DIRECT®
Thin Solid Films 496 (2006) 273 – 280
thin solid films
www.elsevier.com/locate/tsf

Preparation, characterization and photocatalytic activity of in situ Fe-doped TiO_2 thin films

Jiaguo Yu [a,*], Huogen Yu [a], C.H. Ao [b], S.C. Lee [b], Jimmy C. Yu [c], Wingkei Ho [c]

[a] *State Key Laboratory of Advanced Technology for Material Synthesis and Processing, Wuhan University of Technology, Wuhan, 430070, P. R. of China*
[b] *Department of Civil and Structural Engineering, Research Center for Urban Environmental Technology and Management, The Hong Kong Polytechnic University, Hung Hom, Kowloon, China*
[c] *Department of Chemistry, The Chinese University of Hong Kong, Shatin, New Territories, Hong Kong, China*

Received 8 November 2004; received in revised form 29 June 2005; accepted 24 August 2005
Available online 3 October 2005

Abstract

Fe-doped TiO_2 thin films were prepared in situ on stainless steel substrates by liquid phase deposition, followed by calcination at various temperatures. It was found that some Fe^{3+} ions were in situ doped into the TiO_2 thin films. At 400 °C, the film became photoactive due to the formation of anatase phase. At 500 °C, the film showed the highest photocatalytic activity due to an optimal Fe^{3+} ion concentration in the film. At 900 °C, the photocatalytic activity of the films decreased significantly due to the further increase of Fe^{3+} ion concentration, the formation of rutile phase and the sintering and growth of TiO_2 crystallites.

PACS: 68.55.-a; 78.66.-w
Keywords: Titanium oxide; Photocatalysis; Steel; X-ray diffraction

1. Introduction

Heterogeneous photocatalysts with high activities have attracted more and more attention in recent years owing to their environmental applications such as air purification, water disinfection, hazardous waste remediation, and water purification [1–9]. Among various oxide semiconductor photocatalysts, titania is the most widely used because of its strong oxidizing power, nontoxicity and long-term photostability. However, the application of powdered TiO_2 in wastewater treatment is limited since a post-treatment separation is required to recover the catalyst. Mobile photocatalyst powder is also not applicable for air purification, as it may contribute to respirable particles that cause adverse human health problems [10]. In order to avoid the use of photocatalyst powders, efforts have been made to coat TiO_2 thin films on various substrates.

Stainless steel is an essential material in buildings due to its high mechanical strength and relatively high resistance to chemical corrosion. This building material can become self-cleaning and air-purifying with a layer of TiO_2 coating. Stainless steel has been used as a supporting substrate for the TiO_2 film photocatalyst prepared by electrophoretic deposition [11–13], metalorganic chemical vapor deposition (MOCVD) [14,15] and sol–gel methods [16–19]. However, the above methods have some disadvantages for industrial applications. The electrophoretic deposition and MOCVD methods require special apparatus for the deposition of TiO_2 films, while the sol–gel method needs repeated coating in order to get a thick film. To solve these drawbacks, a liquid phase deposition (LPD) method has been developed to form titanium dioxide thin films in recent years [20–23]. In the deposition process, metal oxide thin films can deposit onto the immersed substrates via a ligand exchange equilibrium reaction of metal-fluoro-complex ions and F^- consuming reaction by the addition of F^- scavengers such as boric acid or metal aluminum. The LPD method is very simple and does not require any special equipment. Moreover, it can be easily applied to various kinds of substrates with large surface area or complex shapes.

It is well known that the photocatalytic activity of TiO_2 thin film depends strongly on the methods of doping, the amount of

* Corresponding author. Tel.: +86 27 87883610; fax: +86 27 87879468.
E-mail address: jiaguoyu@yahoo.com (J. Yu).

0040-6090/$ - see front matter © 2005 Elsevier B.V. All rights reserved.
doi:10.1016/j.tsf.2005.08.352

doping and the calcination temperatures of samples, since they give a decisive influence on the chemical and physical properties of TiO_2 thin film [10,24]. Therefore, it is necessary to investigate the effects of the doping method, doping content and calcination temperatures on the surface microstructures, compositions and photocatalytic activity of the films. In the present work, we prepared Fe-doped titania thin films on stainless steel substrates from a $(NH_4)_2TiF_6$ aqueous solution upon addition of boric acid by the LPD method. The as-prepared TiO_2 films were then calcined at different temperatures. After that, the photocatalytic activity of the films was evaluated by the photocatalytic oxidation of nitrogen monoxide in the gas phase and the photocatalytic discoloration of methyl orange aqueous solution in the aqueous phase. To the best of our knowledge, this is the first report showing the influences of in situ Fe-doped and calcination temperatures on the microstructure and photocatalytic activity of TiO_2 films deposited on stainless steel substrate via the LPD method. This work may provide new insights into the preparation of highly photoactive TiO_2 thin films.

2. Experimental details

2.1. Preparation of in situ Fe-doped TiO_2 thin film

The aqueous solutions of ammonium hexafluorotitanate and boric acid were mixed, stirred and used as the treatment solution. The concentrations of ammonium hexafluorotitanate and boric acid in the treatment solution were 0.1 mol L^{-1} and 0.3 mol L^{-1}, respectively, which are in the concentration range where transparent films can be obtained [25]. The stainless steel substrates were immersed vertically into the treatment solution for 48 h. After the substrates were taken out and rinsed with distilled water, the TiO_2 thin films were calcined at 100, 300, 400, 500, 600, 700, 800 and 900 °C in air for 1 h, respectively.

2.2. Characterization

Infrared absorption spectra were recorded with a Fourier transform infrared spectroscopy (FTIR) spectrometer (Nialet-60SXB, American) using KBr disks containing powdered samples of the films obtained by scratching the films off the substrates. The X-ray diffraction (XRD) patterns obtained on a Bruker D8 Advance X-ray diffractometer using Cu-Kα radiation at a scan rate of 0.05° $2\theta \cdot S^{-1}$ were used to determine the identity of crystalline phase and the crystallite size. The accelerating voltage and the applied current were 40 kV and 40 mA, respectively. The surface morphologies and thickness of TiO_2 thin films were observed using scanning electron microscopy (SEM) (type JSM-5610LV) with an accelerating voltage of 20 kV. Photoluminescence spectra (PL) were obtained at room temperature on a SHIMADZU RF-5301 PC spectrometer using a 300 nm excitation light. X-ray photoelectron spectroscopy (XPS) measurements were performed on a Kratos XSAM800 XPS system equipped with two ultrahigh-vacuum (UHV) chambers. The pressure in the chambers during the experiments was about 10^{-7} Pa and an Mg-Kα X-ray source was used. The analyzer was operated at 20 eV pass energy for high-resolution spectra and 50 eV for survey spectra. All the binding energies were referenced to the C1s peak at 284.8 eV of the surface adventitious carbon.

2.3. Photocatalytic oxidation of NO in a gas phase

The evaluation of photocatalytic activity of the thin films in the gas phase was performed by measuring the photodegradation of NO, which was fed to a laboratory-scale continuous flow photoreactor. The inlet concentration of NO is 200 ppb. The detailed experimental setup and process have been reported elsewhere [26,27]. A reactor with a volume of 18.6 L (20.1 $H \times 44.2$ $L \times 21$ W cm) and surface coated with a teflon film (BYTAC Type AF-21) was used for this study. A 6 W 365 nm UV lamp (Cole-Parmer Instrument Co. USA) was used as light source and its intensity was determined with a UV meter (Spectroline DRC-100X). The UV lamp was horizontally placed at the upper part of the reactor, 14 cm from both ends. The UV intensity measured in all experiments was 600 μW/cm^2. The TiO_2 film sample was supported by a teflon film and fixed horizontally at a vertical distance of 5 cm away from the UV lamp. Stainless steel sampling ports and teflon tubing were used to connect the reactor and the analytical instruments. A zero air generator (Thermo Environmental Inc., Model 111) was used to supply the air stream. The desired humidity of the flow was controlled by passing the zero air stream through a humidification chamber. The reactant stream and the zero air streams were pre-mixed in a gas blender (Advanced Pollution Instrumentation Inc., Model 700) and a mass flow controller controlled the desired flow. After the inlet and the outlet concentration of the target pollutants achieved equilibrium (30 min), the UV lamp was turned on and initiated the reaction. The concentration of NO was continuously measured by a Chemiluminescence NO analyzer (Thermo Environmental Instruments Inc. Model 42c), which monitored NO, NO_2, and NO_x with a sampling rate of 0.7 L/min. The photocatalytic activity of Fe-doped TiO_2 thin film was characterized by the removal rate of NO. The removal (%) was calculated as follows [26]:

$$\textit{removal}\ (\%) = \frac{\textit{initial concentration} - \textit{final concentration}}{\textit{initial concentration}} \times 100\% \quad (1)$$

where initial concentration is the inlet NO concentration and final concentration is the outlet NO concentration measured at 120 min after the UV lamp was turned on.

2.4. Photocatalytic discoloration of methyl orange in an aqueous phase

The photocatalytic activity of the Fe-doped TiO_2 thin films was evaluated by the photocatalytic discoloration of methyl orange solution at ambient temperature. Experimental details were as follows: Fe-doped thin films were settled in a 25 mL

methyl orange solution with a concentration of 1.53×10^{-3} mol L^{-1} in a glass cell (16 $L \times 6$ $W \times 3$ H cm). The area of the film used for each experiment was kept at 80 cm^2. A 15 W 365 nm UV lamp (Cole-Parmer Instrument Co.) was used as the light source. One face of the thin films was irradiated along the normal direction. The average light intensity striking on the film was about 112 μW cm^{-2}, as measured by a UV meter with the peak intensity of 365 nm. The concentration of methyl orange was determined by UV-visible spectrometry. As the concentration of methyl orange solution was low, its photocatalytic discoloration process is a pseudo-first-order reaction, which kinetics can be expressed as: $\ln(c_0/c)=kt$, where k is the apparent rate constant and c_0 and c are the methyl orange concentrations at $t=0$ and $t=t$, respectively [24].

3. Results and discussion

3.1. FTIR spectroscopy

FTIR spectra of the TiO_2 thin films are shown in Fig. 1. A broad absorption peak at 400–700 cm^{-1} wavelength ranges is clearly visible. This is attributed to Ti–O stretching and Ti–O–Ti bridging stretching modes [28]. The absorption peak at 910 cm^{-1} is due to the vibration of Ti–F bond [29]. The peaks at 1419 cm^{-1} and at 1638 cm^{-1} can be ascribed to the bending vibrations of N–H bonds and O–H bonds, respectively [30,31]. A broad band is observed at 2800–3800 cm^{-1} wavelength ranges, which is assigned to the stretching modes of O–H bonds and of N–H bonds [31,32]. The FTIR spectra of the sample dried at 100 °C reveals that the Ti–O, Ti–F, N–H, O–H groups exist in the as-prepared sample. Since the LPD process was performed in an aqueous solution system, the samples easily adsorbed water molecules, NH_4^+ and F^- ions in the treatment solution. With increasing calcination temperature, the intensities of peaks related to the O–H, N–H, and Ti–F groups gradually decreased and the N–H and Ti–F groups then disappeared completely at 500 °C, while the intensities of peak related to Ti–O group increased. It has been shown that the removal of N–H, Ti–F and O–H groups promoted the rearrangement of Ti–O network and enhanced the crystallization of titania. When calcination temperature was over 500 °C, there were also some small vibration bands related to the O–H bonds, which was caused by the chemically adsorbed water of Ti–OH. This meant that the chemisorbed water was not completely removed even at 900 °C.

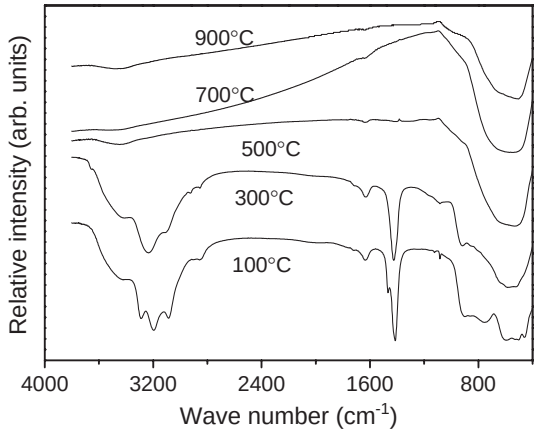

Fig. 1. Infrared spectra of TiO_2 powder calcined at 100, 300, 500, 700 and 900 °C.

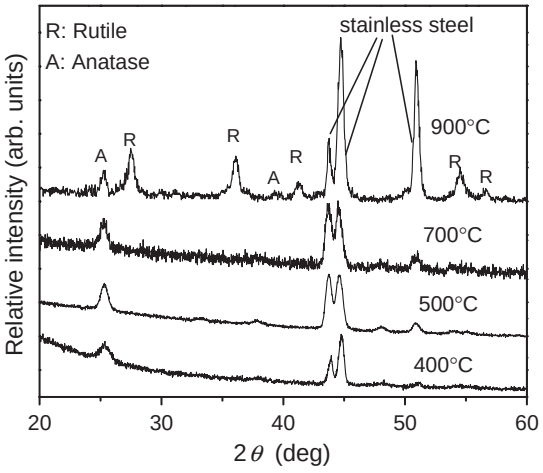

Fig. 2. XRD patterns of Fe-doped TiO_2 thin films calcined at 400, 500, 700 and 900 °C.

3.2. XRD study

XRD was used to investigate the phase structures of the TiO_2 films. When calcination temperature was below 400 °C, there was no diffraction peak (not shown here). This was due to the fact that the thin films were amorphous. Fig. 2 shows the XRD patterns of the Fe-doped TiO_2 thin films calcined at 400, 500, 700, and 900 °C. At 400 °C, a weak diffraction peak at $2\theta=25.3°$ was observed. This suggested that the phase transformation temperature from amorphous to anatase in the thin films was ca. 400 °C. With increasing calcination temperature, the peak intensity of anatase increased and the width of (101) peak of anatase became narrower. This was due to the enhancement of crystallization and the growth of crystallites. At 900 °C, the rutile phase began to form and became the predominant crystallite phase. Therefore, the phase transformation temperature of anatase to rutile was ca. 900 °C for the Fe-doped TiO_2 thin films prepared by the LPD method. Such a transformation temperature was higher than that of the samples prepared by the sol–gel method (ca. 700 °C) [9,24]. The higher phase transformation temperature from anatase to rutile can be ascribed to the formation of Ti–O–Fe bonds in the thin film (as discussed below). The Fe–O species at the interface of TiO_2 crystallites inhibited the formation of the rutile phase by preventing the nucleation that was necessary for the phase transformation to rutile. Therefore, it was necessary to provide greater heat to promote the phase transformation of anatase to rutile. The similar results were observed in the TiO_2 thin films deposited on the fused quartz by the LPD method [6].

3.3. SEM analysis

Fig. 3 shows the SEM micrographs of the Fe-doped TiO_2 thin films calcined at 100, 300, 500, 700 and 900 °C. The surface morphologies and roughness of the Fe-doped TiO_2 thin films did not change significantly as long as the calcination temperature was kept below 700 °C. With increasing calcination temperature, the cracks on the surface of the films become wider and more cracks were observed. This was caused by the different thermal expansion coefficient between the TiO_2 and the stainless steel substrate. The stainless steel substrate had a higher coefficient (17×10^{-6} °C) of line thermal expansion than that of TiO_2 ($2.1–2.8 \times 10^{-6}$ °C) [18]. The different thermal expansion coefficients between TiO_2 and the stainless steel substrate also caused interfacial stresses between the thin film and the substrates. During heating or cooling, if the interfacial stresses were larger than the adhering stresses between the thin film and the substrate, the film would drop off from the substrate. In our samples, no such phenomenon was observed. The strong adhesion between the films and stainless steel was attributed to the formation of the chemical bonds of Ti–O–Fe at the interface of TiO_2 and substrate during calcination. Hence, heat treatment not only enhanced the crystallization of TiO_2 thin films but also improved the adhesion between the TiO_2 thin film and the stainless steel substrate. At 900 °C, the surface morphology of the TiO_2 thin film changed significantly. As seen from Fig. 3(e), the width of cracks increased significantly and the TiO_2 film was composed of many large crystallites with a diameter of 200–400 nm. This was attributed to the fact that the phase transition from anatase to rutile accelerated the grain growth and sintering of TiO_2 crystallites by providing the heat of phase transformation. The thickness of Fe-doped TiO_2 thin films calcined at 100, 500, 700 and 900 °C were ca. 400, 320, 250 and 230 nm, respectively, according to the SEM cross-section observation of the films.

3.4. Photoluminescence spectra

PL emission spectra can be used to investigate the efficiency of charge carrier trapping, immigration and transfer, and to understand the fate of photo-generated electrons and holes in semiconductor since PL emission results from the recombination of free carriers [33,34]. Fig. 4 shows the room temperature PL spectra for Fe-doped TiO_2 thin films calcined at 100, 300, 500, 700 and 900 °C in the range of 2.3–3.6 eV. Two main emission peaks appear at about 3.38 and 2.62 eV, which correspond to the 367 and 473 nm wavelengths, respectively. The former is ascribed to the emission of band gap transition [35]. The latter is the emission signal originated from the charge-transfer transition from Ti^{3+} to oxygen anion

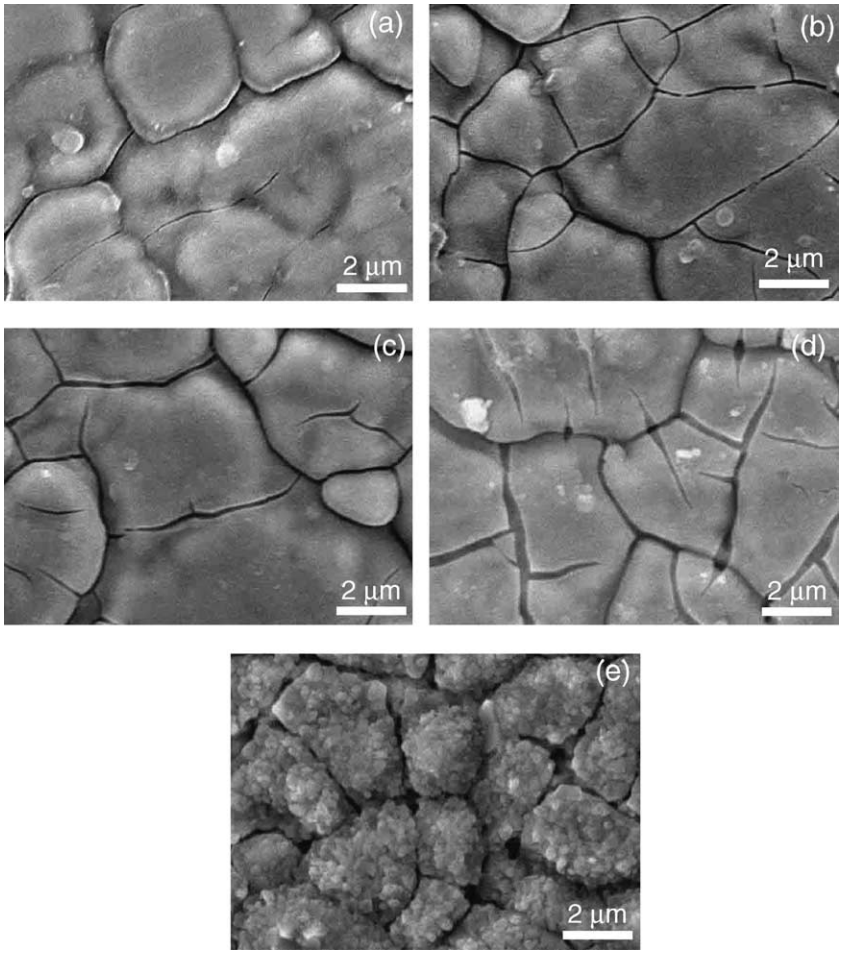

Fig. 3. SEM micrographs of Fe-doped TiO_2 films calcined at (a) 100, (b) 300, (c) 500, (d) 700 and (e) 900 °C.

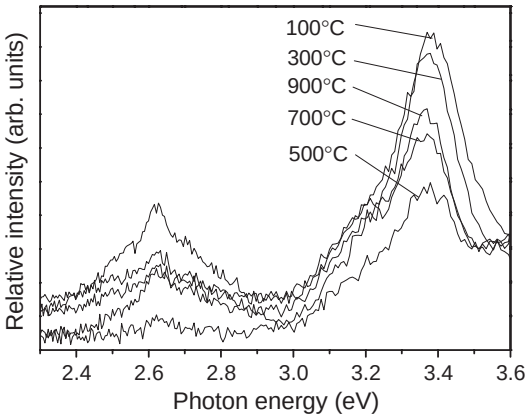

Fig. 4. PL spectra of Fe-doped TiO_2 thin films calcined at 100, 300, 500, 700 and 900 °C.

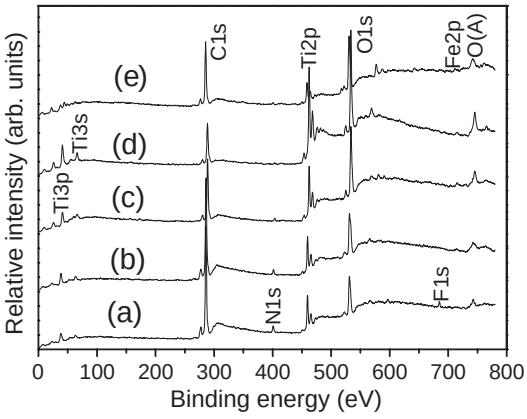

Fig. 5. XPS survey spectra for the surface of Fe-doped TiO_2 films calcined at (a) 100, (b) 300, (c) 500, (d) 700 and (e) 900 °C.

in a TiO_6^{8-} complex [35,36]. The difference of about 0.76 eV between the band gap energy (3.38 eV) and the emission peak energy (2.62 eV) is caused by the Stokes shift due to the Franck–Condon effect [35,37,38]. The variation of PL intensity may result from the change of defect states on the shallow level of film surface [34,39]. Therefore, a lower PL intensity might show a lower recombination rate of photo-generated electrons and holes on the shallow level of film under light irradiation. It can be seen from Fig. 4 that the PL intensity decreased with increasing calcination temperature. At 500 °C, the PL intensity reached its lowest value and then increased at a calcination temperature of higher than 500 °C. Below 500 °C, the decrease of PL intensity was due to the decomposition of intermediates $(NH_4)_2TiF_{6-n}(OH)_n$, removal of other impurities, phase transformation of amorphous to anatase and enhancement of crystallization of anatase, leading to the decrease of defect sites or recombination centers. At 700 °C, the film showed a higher PL intensity compared with the sample calcined at 500 °C. Since the phase composition and surface microstructure (morphology) of the films did not change significantly, the increase of PL intensity could be ascribed to the introduction of new defect sites in the sample due to the immigration of Fe^{3+} from the stainless steel substrates into the films (as shown in Table 1) [34]. These results indicated that when the content of Fe^{3+} ions was high, they became the recombination centers of photogenerated electrons and holes. At 900 °C, the PL emission intensity of thin film further increased. This might be due to the increase of more new defect sites caused by the further increase of the content of Fe^{3+} ions, the phase transformation of anatase to rutile and the formation of cracks in the thin film.

Table 1
Composition (at.%)[a] of Fe-doped TiO_2 thin films calcined at various temperatures according to XPS analysis

Films (°C)	O	Ti	F	Fe	N
100	66	23	5	1	5
300	70	24	1	1	4
500	70	24	0	2	4
700	69	25	0	3	3
900	73	21	0	4	2

[a] The errors in the reported values are estimated to be less than 5%.

3.5. XPS studies

Fig. 5 shows the XPS survey spectra of the Fe-doped TiO_2 thin films calcined at 100, 300, 500, 700 and 900 °C. The Fe-doped TiO_2 thin films deposited on stainless steel contained not only Ti and O elements, but also F, N and Fe. The XPS peak for C1s at E_b=284.8 eV was observed due to the adventitious hydrocarbon from the XPS instrument itself. The XPS peaks for F and N came from the residual elements in the precursor solution. Table 1 shows the composition (at.%) of the Fe-doped TiO_2 thin films calcined at various temperatures according to the XPS analysis. It can be seen that the amount of F and N elements in the film decreased with increasing calcination temperature and finally the F element disappeared completely at 500 °C. Fig. 6 shows the high-resolution XPS spectra of Fe2p region taken on the surface of the Fe-doped TiO_2 thin films calcined at 100, 300, 500, 700 and 900 °C, respectively. It was found from the binding energies that the peak for $Fe2p_{3/2}$ in each Fe-doped TiO_2 film could be attributed to Fe^{3+} [14,17]. It is well known that XPS involves surface probe detecting electrons that are generated from a depth of a few nanometers

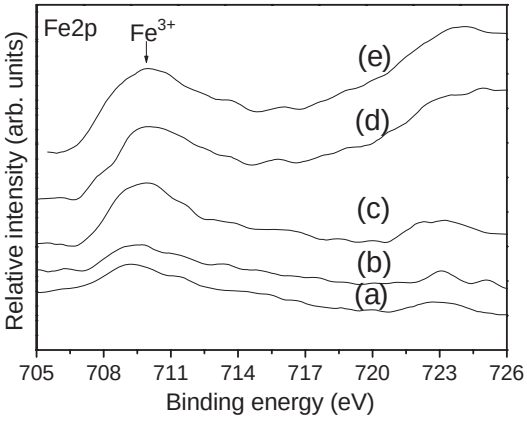

Fig. 6. High-resolution XPS spectra of the Fe2p region of Fe-doped TiO_2 thin films calcined at (a) 100, (b) 300, (c) 500, (d) 700 and (e) 900 °C.

on the surface of sample. The thickness of the TiO_2 thin films in our experiment was over 200 nm, which was much larger than the depth that XPS could detect. Moreover, the film sample calcined at 100 °C was dense according to the previous SEM observation. Therefore, it could be inferred that the photoelectron peaks for the Fe2p came from the thin film itself instead of the surface of the stainless steel substrate. Usually, it is impossible for the Fe^{3+} to diffuse from stainless steel substrate into the TiO_2 thin film at 100 °C. Further experimental observation indicated that the as-prepared sample before calcination also showed the photoelectron peaks for the Fe2p in the XPS spectrum. In our experiment, there was no Fe element in the treatment solution and only a plastic beaker was used as a container and stainless steel as the substrate. Therefore, it could be concluded that the Fe element in the as-prepared films could only come from the stainless steel substrate. During deposition, the ligand exchange equilibrium reactions of metal-fluorocomplex ions and the consuming reaction of F^- ions by boric acid as a F^- scavenger existed in the same reaction system as follows [40,41]:

$$[TiF_6]^{2-} + nH_2O \rightleftharpoons [TiF_{6-n}(OH)n]^{2-} + nHF. \quad (2)$$

$$H_3BO_3 + 4HF \rightleftharpoons BF_4^- + H_3O^+ + 2H_2O. \quad (3)$$

According to Eqs. (2) and (3), HF and H^+ would be produced in the treatment solution during deposition. When the stainless steel substrate was immersed into the treatment solution, the following reaction would occur:

$$Fe + 6HF \rightarrow [FeF_6]^{3-} + 3/2H_2 + 3H^+. \quad (4)$$

If the surface of the stainless steel has been partly oxidized before deposition, the following reaction would also occur in the above reaction system:

$$Fe_2O_3 + 12HF \rightarrow 2[FeF_6]^{3-} + 3H_2O + 6H^+. \quad (5)$$

Two other reactions could also take place [42]:

$$[FeF_6]^{3-} + nH_2O \rightleftharpoons [FeF_{6-n}(OH)_n]^{3-} + nHF \quad (6)$$

$$[FeF_{6-n}(OH)_n]^{3-} + (6-n)H_2O \rightleftharpoons [Fe(OH)_6]^{3-} + (6-n)HF. \quad (7)$$

The ligand-exchange equilibrium reactions (Eqs. (6) and (7)) shifted to the right when the consuming reaction of F^- ions (Eq. (3)) occurred by the addition of boric acid. Since the radius of Fe^{3+} (0.64 Å) and Ti^{4+} (0.68 Å) were similar, the Fe^{3+} could be incorporated into the lattice of TiO_2 to form Ti–O–Fe bonds in the TiO_2 thin film by the dehydration reactions between the $[FeF_{6-n}(OH)_n]^{3-}$ and $[TiF_{6-n}(OH)_n]^{2-}$ ions during deposition and calcination [43]. Similarly, Fe^{2+} could also be deposited in the thin film when there were some Fe^{2+} ions in the treatment solution, but the Fe^{2+} would be easily oxidized to Fe^{3+} during calcination in air. Thus, the Fe element in the TiO_2 thin films existed mainly in the +3 oxidation state (Fe^{3+}). As shown in Table 1 and Fig. 6, the amount of Fe^{3+} increased significantly when the calcination temperature was over 500 °C. Zhu et al. [16] and Yu et al. [19] also reported the presence of Fe in the as-prepared TiO_2 films deposited on stainless steel substrate by the sol–gel method at 500 °C. This was ascribed to the diffusion of Fe element from the stainless steel into the TiO_2 thin films. Herein, there also existed the diffusion phenomenon of Fe element for our samples calcined at 500 °C or a higher temperature.

3.6. Photocatalytic activities of Fe-doped TiO_2 thin films

The photocatalytic activity of the Fe-doped TiO_2 thin films was evaluated by the photocatalytic degradation of NO in the gas phase. Fig. 7 shows the photodegradation of 200 ppb NO for the Fe-doped TiO_2 thin film calcined at 500 °C. Prior to UV illumination, the adsorption and desorption had reached equilibrium. When the UV lamp was turned on, the photodegradation reaction of NO was initiated. The concentration of NO dropped rapidly in the first 10 min and reached the lowest value of 76 ppb. After that, the concentration of NO increased slowly with increasing irradiation time, which was ascribed to the accumulation of a small amount of HNO_3 on the surface of the films, leading to the deactivation of the Fe-doped TiO_2 thin films [26,44]. After 120 min, the concentration of NO steadily reached a photo-steady-state concentration of 105 ppb.

Fig. 8 shows the effects of calcination temperatures on the removal of NO for the Fe-doped TiO_2 thin films. There was no photocatalytic activity (or negligible) for the Fe-doped TiO_2 thin films obtained at below 400 °C. This was attributed to the fact that the thin films were composed of amorphous TiO_2. At 400 °C, the film showed obvious photocatalytic activity due to the formation of anatase. With increasing calcination temperature, the photocatalytic activity of thin films increased obviously and reached a maximum value at 500 °C. Then the photocatalytic activity decreased steadily with a further increase in calcination temperature. At 900 °C, the film showed the lowest photoreaction activity. From 400 to 500 °C, the increase of the photocatalytic activity of the films was ascribed not only to the enhancement of crystallization of anatase (as shown in Fig. 2) but also to the increase of the Fe^{3+} concentration (as shown in Table 1 and Fig. 6). It is well known

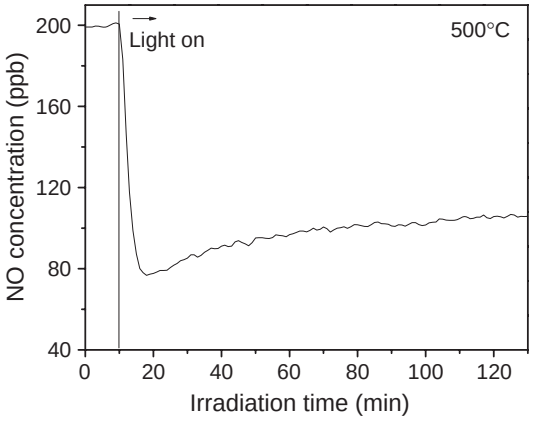

Fig. 7. The photodegradation of NO for the Fe-doped TiO_2 thin film sample calcined at 500 °C. Residence time 3.72 min, humidity levels 2200 ppmv, 200 ppb NO.

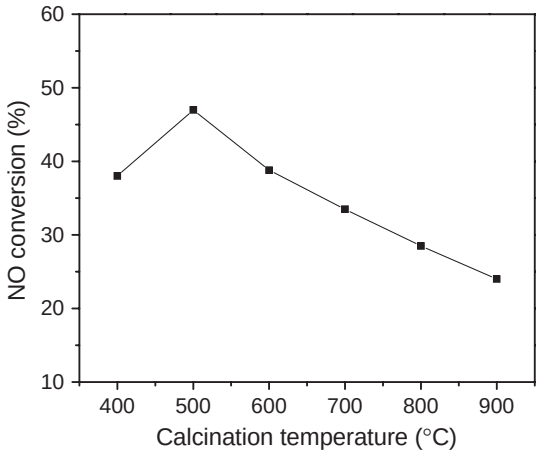

Fig. 8. The removals of NO for the Fe-doped TiO_2 thin films calcined at different calcination temperatures. Residence time 3.72 min, humidity levels 2200 ppmv, 200 ppb NO.

that a small amount of Fe^{3+} ions can act as the trap sites of both photo-generated holes and electrons and inhibit the hole–electron recombination [19,45–50]:

$$TiO_2 + h\nu \rightarrow h^+ + e^- \text{ charge pair generation} \quad (8)$$

$$Ti^{4+} + e^- \rightarrow Ti^{3+} \quad (9)$$

$$O^{2-} + h^+ \rightarrow O^- \quad (10)$$

$$Fe^{3+} + Ti^{3+} \rightarrow Fe^{2+} + Ti^{4+} \text{ electron trap} \quad (11)$$

$$Fe^{3+} + O^- \rightarrow Fe^{4+} + O^{2-} \text{ hole trap.} \quad (12)$$

From the viewpoint of crystal field theory, Fe^{4+} and Fe^{2+} ions are relatively unstable as compared to Fe^{3+} ions, which have half-filled d orbitals (d^5) [19,49]. Therefore, there is a tendency for the transfer of the trapped charges from Fe^{4+} and Fe^{2+} to the film surface to initiate the following reactions [19,49]:

$$Fe^{4+} + OH^- \rightarrow Fe^{3+} + OH\bullet \text{ hole release} \quad (13)$$

$$Fe^{2+} + O_2 \rightarrow Fe^{3+} + O_2^- \text{ electron release.} \quad (14)$$

Accordingly, the increase of Fe^{3+} dopant concentration in the film at 500 °C was also responsible for an increase in its photocatalytic activity.

Many investigations have shown that the photocatalytic activity of Fe-doped TiO_2 is strongly dependent on the dopant concentration, and more Fe^{3+} results in an increase of recombination rate of photo-generated electrons and holes and a decrease of photocatalytic activity [45,51]. When the Fe^{3+} concentration exceeded an optimal dopant concentration, the Fe^{3+} ions steadily became the recombination centers of photo-generated electrons and holes. This was ascribed to the fact that more Fe^{3+} sites would trap more photo-generated electrons and holes, but the trapped free carrier pairs easily recombined through quantum tunneling [52]. Moreover, when the amount of Fe^{3+} was large, there were more Fe^{3+}-associated sites in the thin films, resulting in a shorter transferring distance between the two activity sites. Therefore, the chance of multiple trappings increased for a free carrier and the transferring time of free carriers from the interior to the surface became longer, leading to the increase of recombination rate. It was clear that the more the Fe^{3+} in the samples, the easier the reactions of recombination happen. Maruska and Ghosh [53] attributed the differences in photocatalytic activity between Fe^{3+}/TiO_2 and Cr^{3+}/TiO_2 to the different diffusion lengths of free carriers. They concluded that the diffusion length for Fe^{3+}/TiO_2 was longer than that for Cr^{3+}/TiO_2, resulting in a higher photoactivity for the Fe^{3+}/TiO_2 sample. Thus, an optimal Fe^{3+} dopant concentration should be expected to exist in our case. Therefore, it was not surprising that the sample calcined at 700 °C showed a lower photocatalytic activity due to the increase of Fe^{3+} concentration that exceeded an optimal Fe^{3+} dopant concentration, although the film exhibited better crystallization compared to the sample obtained at 500 °C. At 900 °C, the film showed the lowest photocatalytic activity. This was attributed to the results of the further increase of Fe^{3+} concentration, the phase transformation of anatase to rutile and the sintering and growth of TiO_2 crystallite [6].

We have reported that the TiO_2 thin films deposited on fused quartz and calcined at 700 °C showed the highest photocatalytic activity for the photocatalytic degradation of methyl orange in an aqueous solution [6], while the TiO_2 thin film deposited on stainless steel and calcined at 500 °C showed the greatest photodegradation rate for NO in the gas phase. The difference in photocatalytic activity for the samples deposited on fused quartz and stainless steel could be ascribed to the influence of Fe dopant on the photocatalytic activity of the TiO_2 thin films. To further evaluate the photocatalytic properties of the Fe-doped TiO_2 thin films deposited on the stainless steel, the photo-degradation of methyl orange was also performed [54]. Fig. 9 shows the relationship between the apparent rate constants of methyl orange degradation and the calcinations temperature. Samples calcined below 400 °C were not photocatalytically active. With increasing calcination temperature, the apparent rate constant increased. At 500 °C, the photocatalytic activity of the sample reached a maximum value of 9.30×10^{-4} min^{-1}. At a higher temperature, it steadily decreased and reached a minimum value of 2.83×10^{-4} min^{-1} at 900 °C. It can be seen

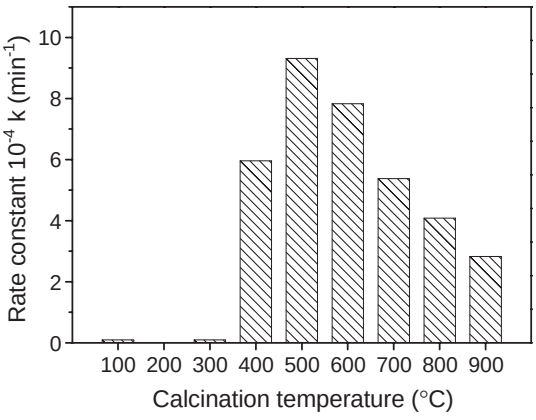

Fig. 9. The effects of calcination temperatures on apparent rate constant of Fe-doped TiO_2 thin films for the photocatalytic discoloration of methyl orange solution in the aqueous phase.

from the above results that the Fe-doped TiO_2 films obtained by the LPD method showed similar photocatalytic activities for both nitrogen monoxide in the gas phase and methyl orange in the aqueous phase. This further confirmed that the sample calcined at 500 °C possessed the highest photocatalytic activity.

4. Conclusions

In situ Fe-doped titania thin films could be deposited on stainless steel substrates by a LPD method. The as-prepared Fe-doped TiO_2 thin films contained not only Ti and O elements, but also a small amount of F, N and Fe. The F and N elements came from the precursor solution and their amounts decreased with increasing calcinations temperature. The Fe^{3+} ions in the Fe-doped TiO_2 thin film came from the $[FeF_{6-n}(OH)_n]^{3-}$ ions formed by a reaction between the treatment solution and the stainless steel substrate and from the diffusion of Fe element from the surface of stainless steel substrate into the thin films during calcination at temperatures $\geq$500 °C.

The photocatalytic activity of the Fe-doped TiO_2 thin films depended strongly on the calcination temperature and the Fe dopant level. At 500 °C, the film exhibited the highest photocatalytic activity. This was ascribed to the fact that an optimal Fe^{3+} concentration was obtained in the film, effectively reducing the recombination of photo-generated free carriers.

Acknowledgements

This work was partially supported by the National Natural Science Foundation of China (50272049 and 20573059). This work was also financially supported by the Excellent Young Teachers Program of MOE of China and Project-Sponsored by SRF for ROCS of SEM of China. The authors would like to thank Department of Civil and Structural Engineering, the Hong Kong Polytechnic University for technical support.

References

[1] K. Honda, A. Fujishima, Nature 238 (1972) 37.
[2] H. Tada, M. Yamamoto, S. Ito, Langmuir 15 (1999) 3699.
[3] H. Liu, S. Cheng, M. Wu, H. Wu, J. Zhang, W. Li, C. Cao, J. Phys. Chem., A 104 (2000) 7016.
[4] M.R. Hoffmann, S.T. Martin, W. Choi, D.W. Bahnemann, Chem. Rev. 95 (1995) 69.
[5] M.A. Fox, M.T. Dulay, Chem. Rev. 93 (1993) 341.
[6] J.G. Yu, H.G. Yu, B. Cheng, X.J. Zhao, J.C. Yu, W.K. Ho, J. Phys. Chem., B 107 (2003) 13871.
[7] J.C. Zhao, T.X. Wu, K.Q. Wu, K. Oikawa, H. Hidaka, N. Serpone, Environ. Sci. Technol. 32 (1998) 2394.
[8] Y.M. Xu, C.H. Langford, Langmuir 17 (2001) 897.
[9] J.G. Yu, J.G. Yu, W.K. Ho, L.Z. Zhang, Chem. Commun. (2001) 1942.
[10] P.H. McMurry, Atmos. Environ. 34 (2000) 1959.
[11] A.H.C. Chan, J.F. Porter, J.P. Barford, C.K. Chan, J. Mater. Res. 17 (2002) 1758.
[12] A. Fernandez, G. Lassaletta, V.M. Jimenez, A. Justo, A.R. Gonzalez-Elipe, J.M. Herrmann, H. Tahiri, Y. Ait-Ichou, Appl. Catal., B Environ. 7 (1995) 49.
[13] J.M. Herrmann, H. Tahiri, C. Guillard, P. Pichat, Catal. Today 54 (1999) 131.
[14] M. Kang, J.H. Lee, S.H. Lee, C.H. Chung, K.J. Yoon, K. Ogino, S. Miyata, S.J. Choung, J. Mol. Catal., A Chem. 193 (2003) 273.
[15] W. Li, S.I. Shah, M. Sung, C.P. Huang, J. Vac. Sci. Technol., B 20 (2002) 2303.
[16] Y.F. Zhu, L. Zhang, L. Wang, Y. Fu, L.L. Gao, J. Mater. Chem. 11 (2001) 1864.
[17] L. Zhang, Y.F. Zhu, Y. He, W. Li, H.B. Sun, Appl. Catal., B Environ. 40 (2003) 287.
[18] G. Balasubramanian, D.D. Dionysiou, M.T. Suidan, Y. Subramanian, I. Baudin, J.M. Laine, J. Mater. Sci. 38 (2003) 823.
[19] J.C. Yu, W.K. Ho, J. Lin, H. Yip, P.K. Wong, Environ. Sci. Technol. 37 (2003) 2296.
[20] H. Nagayama, H. Honda, H. Kawahara, J. Electrochem. Soc. 135 (1988) 2013.
[21] H. Pizem, C.N. Sukenik, U. Sampathkumaran, A.K. Mcllwain, M.R. De Guire, Chem. Mater. 14 (2002) 2476.
[22] Y. Masuda, S. Ieda, K. Koumoto, Langmuir 19 (2003) 4415.
[23] A. Dutschke, C. Diegelmann, P. Lobmann, J. Mater. Chem. 13 (2003) 1058.
[24] J.G. Yu, X.J. Zhao, Mater. Res. Bull. 36 (2001) 97.
[25] S. Deki, Y. Aoi, O. Hiroi, A. Kajinami, Chem. Lett. 6 (1996) 433.
[26] C.H. Ao, S.C. Lee, Appl. Catal., B Environ. 44 (2003) 191.
[27] C.H. Ao, S.C. Lee, C.L. Mak, L.Y. Chan, Appl. Catal., B Environ 42 (2003) 119.
[28] A.M. Peiro, J. Peral, C. Domingo, X. Momenech, J.A. Ayllon, Chem. Mater. 13 (2001) 2567.
[29] K. Tsukma, T. Akiyama, N. Yamada, H. Imai, J. Non-Cryst. Solids 231 (1998) 161.
[30] J.G. Yu, J.C. Yu, X.J. Zhao, J. Sol–Gel Sci. Technol. 24 (2002) 95.
[31] H.Y.Y. Ko, M. Mizuhata, A. Kajinami, S. Deki, J. Fluorine Chem. 120 (2003) 157.
[32] M. Macek, B. Orel, U.O. Krasorec, J. Electrochem. Soc. 28 (1983) 17.
[33] X.Z. Li, F.B. Li, Environ. Sci. Technol. 35 (2001) 2381.
[34] F.B. Li, X.Z. Li, Appl. Catal., A Gen. 228 (2002) 15.
[35] F.B. Li, X.Z. Li, Chemosphere 48 (2002) 1103.
[36] J.C. Yu, J.G. Yu, W.K. Ho, Z.T. Jiang, L.Z. Zhang, Chem. Mater. 14 (2002) 3808.
[37] K. Fujihara, S. Izumi, T. Ohno, M. Matsumura, J. Photochem. Photobiol., A Chem. 132 (2000) 99.
[38] N. Serpone, D. Lawless, R. Khairutdinov, J. Phys. Chem. 99 (1995) 16646.
[39] T. Toyoda, T. Hayakawa, K. Abe, T. Shigenari, Q. Shen, J. Lumin. 87–89 (2000) 1237.
[40] R.H. Schmitt, E.L. Glove, R.D. Brown, J. Am. Chem. Soc. 82 (1960) 5292.
[41] C.A. Wamser, J. Am. Chem. Soc. 73 (1951) 409.
[42] S. Deki, Y. Aoi, J. Okibe, H. Yanagimoto, A. Kajinami, M. Mizuhata, J. Mater. Chem. 7 (1997) 1769.
[43] C.Y. Wang, C. Bottcher, D.W. Bahnemann, J.K. Dohrmann, J. Mater. Chem. 13 (2003) 2322.
[44] I. Ibusuki, K. Takeuchi, J. Mol. Catal. 88 (1994) 93.
[45] M. Graetzel, R.F. Howe, J. Phys. Chem. 94 (1990) 2566.
[46] M.I. Litter, J.A. Navio, J. Photochem. Photobiol., A Chem. 98 (1996) 171.
[47] F.S. Varveri, A.E. Mantaka-Marketou, K. Papadopoulos, J. Nikokavouras, J. Photochem. Photobiol., A Chem. 56 (1991) 113.
[48] J. Soria, J.C. Conesa, V. Augugliaro, L. Palmisano, M. Schiavello, A. Schafani, J. Phys. Chem. 95 (1991) 274.
[49] W. Choi, A. Termin, M.R. Hoffmann, J. Phys. Chem. 98 (1994) 13669.
[50] K. Mizushima, M. Tanaka, A. Asai, S. Iida, J. Phys. Chem. Solids 40 (1979) 1129.
[51] J.A. Navio, F.J. Marchena, M. Roncel, M.A. De La Rosa, J. Photochem. Photobiol., A Chem. 55 (1991) 319.
[52] Z.B. Zhang, C.C. Wang, R. Zakaria, J.Y. Ying, J. Phys. Chem., B 102 (1998) 10871.
[53] H.P. Maruska, A.K. Ghosh, Sol. Energy Mater. 1 (1979) 237.
[54] J.G. Yu, X.J. Zhao, Q.N. Zhao, Thin Solid Films 379 (2000) 7.